

¹ High-level cognition is supported by information-rich but
² compressible brain activity patterns

3 Lucy L. W. Owen^{1,2} and Jeremy R. Manning^{1,*}

¹Department of Psychological and Brain Sciences,
Dartmouth College, Hanover, NH

²Carney Institute for Brain Sciences,
Brown University, Providence, RI

* Address correspondence to jeremy.r.manning@dartmouth.edu

December 20, 2023

5 Abstract

We applied dimensionality reduction algorithms and pattern classifiers to functional neuroimaging data collected as participants listened to a story, temporally scrambled versions of the story, or underwent a resting state scanning session. These experimental conditions were intended to require different depths of processing and inspire different levels of cognitive engagement. We considered two primary aspects of the data. First, we treated the maximum achievable decoding accuracy across participants as an indicator of the “informativeness” of the recorded patterns. Second, we treated the number of features (components) required to achieve a threshold decoding accuracy as a proxy for the “compressibility” of the neural patterns (where fewer components indicate greater compression). Overall, we found that the peak decoding accuracy (achievable without restricting the numbers of features) was highest in the intact (unscrambled) story listening condition. However, the number of features required to achieve comparable classification accuracy was also lowest in the intact story listening condition. Taken together, our work suggests that our brain networks flexibly reconfigure according to ongoing task demands, and that the activity patterns associated with higher-order cognition and high engagement are both more informative and more compressible than the activity patterns associated with lower-order tasks and lower levels of engagement.

Keywords: information, compression, temporal decoding, dimensionality reduction, neuroimaging

²⁴ Introduction

25 Large-scale networks, including the human brain, may be conceptualized as occupying one or
26 more positions along on a continuum. At one extreme, every node is fully independent from
27 every other node. At the other extreme, all nodes behave identically. Each extreme optimizes
28 key properties of how the network functions. When every node is independent, the network is

29 maximally *expressive*: if we define the network’s “state” as the activity pattern across its nodes, then
30 every state is equally reachable by a network with fully independent nodes. On the other hand, a
31 network of identically behaved nodes optimizes *robustness*: any subset of nodes may be removed
32 from the network without any loss of function or expressive power, as long as any single node
33 remains. Presumably, most natural systems tend to occupy positions between these extremes. We
34 wondered: might the human brain reconfigure itself to be more flexible or more robust according
35 to ongoing demands? In other words, might the brain reconfigure its connections or behaviors
36 under different circumstances to change its position along this continuum?

37 Closely related to the above notions of expressiveness versus robustness are measures of
38 how much *information* is contained in a given signal or pattern, and how *redundant* a signal
39 is (Shannon, 1948). Formally, information is defined as the amount of uncertainty about a given
40 variables’ outcomes (i.e., entropy), measured in *bits*, or the optimal number of yes/no questions
41 needed to reduce uncertainty about the variable’s outcomes to zero. Highly complex systems with
42 many degrees of freedom (i.e., high flexibility and expressiveness), are more information-rich than
43 simpler or more constrained systems. The redundancy of a signal denotes the difference between
44 how expressive the signal *could* be (i.e., proportional to the number of unique states or symbols
45 used to transmit the signal) and the actual information rate (i.e., the entropy of each individual
46 state or symbol). If a brain network’s nodes are fully independent, then the number of bits required
47 to express a single activity pattern is proportional to the number of nodes. The network would
48 also be minimally redundant, since the status of every node would be needed to fully express a
49 single brain activity pattern. If a brain network’s nodes are fully coupled and identical, then the
50 number of bits required to express a single activity pattern is proportional to the number of unique
51 states or values any individual node can take on. Such a network would be highly redundant,
52 since knowing any individual node’s state would be sufficient to recover the full-brain activity
53 pattern. Highly redundant systems are also robust, since there is little total information loss due
54 to removing any given observation.

55 We take as a given that brain activity is highly flexible: our brains can exhibit nearly infinite
56 varieties of activity patterns. This flexibility implies that our brains’ activity patterns are highly
57 information rich. However, brain activity patterns are also highly structured. For example,
58 full-brain correlation matrices are stable within (Finn et al., 2017, 2015; Gratton et al., 2018) and

59 across (Cole et al., 2014; Glerean et al., 2012; Gratton et al., 2018; Yeo et al., 2011) individuals. This
60 stability suggests that our brains' activity patterns are at least partially constrained, for example
61 by anatomical, external, or internal factors. Constraints on brain activity that limit its flexibility
62 decrease expressiveness (i.e., its information rate). However, constraints on brain activity also
63 increase its robustness to noise (e.g., "missing" or corrupted signals may be partially recovered).
64 For example, recent work has shown that full-brain activity patterns may be reliably recovered
65 from only a relatively small number of implanted electrodes (Owen et al., 2020; Scangos et al.,
66 2021). This robustness property suggests that the relevant signal (e.g., underlying factors that
67 have some influence over brain activity patterns) are compressible.

68 To the extent that brain activity patterns contain rich task-relevant information, we should be
69 able to use the activity patterns to accurately differentiate between different aspects of a task (e.g.,
70 using pattern classifiers; Norman et al., 2006). For example, prior work has shown a direct
71 correspondence between classification accuracy and the information content of a signal (Alvarez,
72 2002). To the extent that brain activity patterns are compressible, we should be able to generate
73 simplified (e.g., lower dimensional) representations of the data while still preserving the relevant
74 or important aspects of the original signal. In general, information content and compressibility
75 are often related but are also dissociable (Fig. 1). If a given signal (e.g., a representation of brain
76 activity patterns) contains more information about ongoing cognitive processes, then the peak
77 decoding accuracy should be high. In the simulations shown in Figure 1C we construct synthetic
78 datasets that have high or low levels of informativeness by varying temporal autocorrelations
79 in the data (see *Synthetic data*). If a signal is compressible, then a low-dimensional embedding
80 of the signal will be similarly informative as the original signal. In the simulations shown in
81 Figure 1C we construct synthetic datasets that have high or low levels of compressibility by
82 varying the covariance structure across features (see *Synthetic data*). As shown in Figure 1D, highly
83 informative datasets yield higher decoding accuracies than less informative datasets (i.e., the peaks
84 of the curves in the top panels of Fig. 1D are higher than the peaks of the curves in the bottom
85 panels). Highly compressible datasets show steeper slopes when we plot decoding accuracy as a
86 function of the number of components used to represent the data (i.e., the slopes of the curves in
87 the left panels of Fig. 1D are steeper than the slopes of the curves in the right panels). Whereas
88 characterizing the informativeness and compressibility of synthetic data can be instructive, we

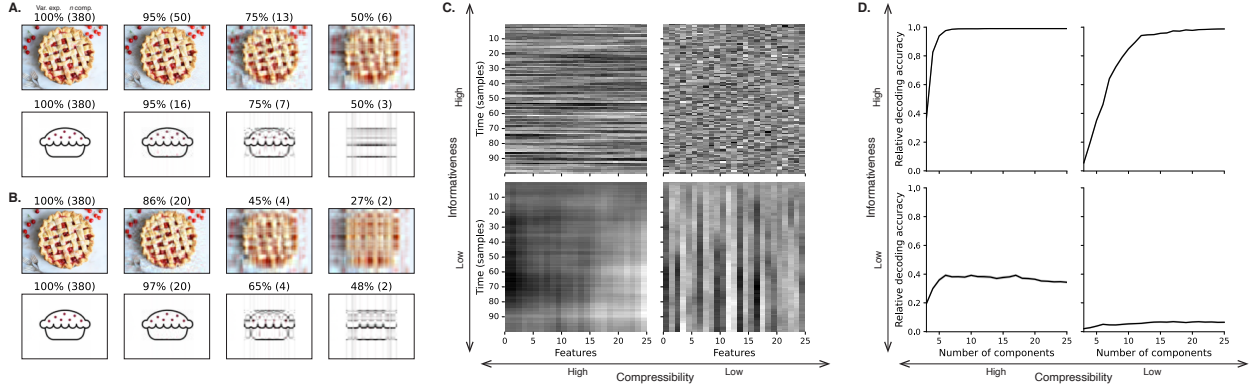


Figure 1: Information content and compressibility. **A. Variance explained for two images.** Consider two example images: a photograph and simple drawing. The images have the same resolutions, but their content is very different. The photograph is more information rich: when we compare the original photograph and drawing (leftmost column), we can see that the photograph captures much more detail. We can also apply principal components analysis to the images, treating the rows of the images as “observations.” Across columns, we identified the numbers of components required to explain 100%, 95%, 75%, or 50% of the cumulative variance in each image (the 100% columns denote the original images). The numbers of components are indicated in parentheses, and the resulting “compressed” images are displayed. This analysis reveals that the drawing is more compressible: just 16 components can explain 95% of the variance in the drawing, whereas 50 components are required to explain 95% of the variance in the photograph. **B. Representing two images with different numbers of components.** Using the same principal component decompositions as in Panel A, we computed the cumulative proportion of variance explained with 380 (original images), 20, 4, or 2 components. This analysis provides another way of characterizing the compressibility of each image by showing that the same number of components can explain more variance in the drawing than in the photograph. **C. Template data from four synthetic datasets.** We constructed four synthetic datasets, each comprising 25 features (columns) observed across 100 samples (rows) from each of 10 simulated “participants.” The datasets were constructed to contain different levels of informativeness and compressibility (see *Synthetic data*). **D. Decoding accuracy by number of components.** For each synthetic dataset, we trained across-participant classifiers to decode timepoint labels. Each panel displays the decoding accuracy as a function of the number of components used to represent the data. Error ribbons denote bootstrap-estimated 95% confidence intervals.

89 are ultimately interested in understanding how these properties relate to brain activity patterns
90 recorded under different cognitive circumstances.

91 Several recent studies suggest that the complexity of brain activity is task-dependent, whereby
92 simpler tasks with lower cognitive demands are reflected by simpler and more compressible brain
93 activity patterns, and more complex tasks with higher cognitive demands are reflected by more
94 complex and less compressible brain activity patterns (Mack et al., 2020; Owen et al., 2021). These
95 findings complement other work suggesting that functional connectivity (correlation) patterns are
96 task-dependent (Cole et al., 2014; Finn et al., 2017; Owen et al., 2020), although see Gratton et
97 al. (2018). Higher-order cognitive processing of a common stimulus also appears to drive more
98 stereotyped task-related activity and functional connectivity across individuals (Hasson et al.,
99 2008; Lerner et al., 2011; Simony & Chang, 2020; Simony et al., 2016).

100 The above studies are consistent with two potential descriptions of how cognitive processes are
101 reflected in brain activity patterns. One possibility is that the information rate of brain activity in-
102 creases during more complex or higher-level cognitive processing. If so, then the ability to reliably
103 decode cognitive states from brain activity patterns should improve with task complexity or with
104 the level (or “depth”) of cognitive processing. A second possibility is that the compressibility of
105 brain activity patterns increases during more complex or higher-level cognitive processing. If so,
106 then individual features of brain recordings, or compressed representations of brain recordings,
107 should carry more information during complex or high-level (versus simple or low-level) cognitive
108 tasks.

109 We used a previously collected neuroimaging dataset to estimate the extent to which each of
110 these two possibilities might hold. The dataset we examined comprised functional magnetic reso-
111 nance imaging (fMRI) data collected as participants listened to an audio recording of a 10-minute
112 story, temporally scrambled recordings of the story, or underwent a resting state scan (Simony
113 et al., 2016). Each of these experimental conditions evokes different depths of cognitive process-
114 ing (Hasson et al., 2008; Lerner et al., 2011; Owen et al., 2021; Simony et al., 2016). We used
115 across-participant classifiers to decode listening times in each condition, as a proxy for how “infor-
116 mative” the task-specific activity patterns were (Simony & Chang, 2020). We also used principle
117 components analysis to generate lower-dimensional representations of the activity patterns. We
118 then repeated the classification analyses after preserving different numbers of components and

119 examined how classification accuracy changed across the different experimental conditions.

120 **Results**

121 We sought to understand whether higher-level cognition is reflected by more reliable and in-
122 formative brain activity patterns, and how compressibility of brain activity patterns relates to
123 cognitive complexity. We developed a computational framework for systematically assessing the
124 informativeness and compressibility of brain activity patterns recorded under different cognitive
125 circumstances. We used across-participant decoding accuracy (see *Forward inference and decoding*
126 *accuracy*) as a proxy for informativeness. To estimate the compressibility of the brain patterns, we
127 used group principal components analysis (PCA) to project the brain patterns into k -dimensional
128 spaces, for different values of k (see *Hierarchical Topographic Factor Analysis (HTFA)* and *Principal*
129 *components analysis (PCA)*). For more compressible brain patterns, decoding accuracy should be
130 more robust to small values of k .

131 We analyzed a dataset collected by Simony et al. (2016) that comprised four experimental con-
132 ditions. These conditions exposed participants to stimuli that systematically varied in cognitive
133 engagement. In the *intact* experimental condition, participants listened to an audio recording of a
134 10-minute Moth Radio Hour story, *Pie Man*, by Jim O’Grady. In the *paragraph*-scrambled experi-
135 mental condition, participants listened to a temporally scrambled version of the story, where the
136 paragraphs occurred out of order, but where the same set of paragraphs was presented over the
137 entire listening interval. All participants in this condition experienced the scrambled paragraphs
138 in the same order. In the *word*-scrambled experimental condition, participants listened to a tem-
139 porally scrambled version of the story, where the words occurred in a random order. Again, all
140 participants in this condition experienced the scrambled words in the same order. Finally, in the
141 *rest* experimental condition, participants lay in the scanner with no overt stimulus, while keeping
142 their eyes open and blinking as needed. This public dataset provided a convenient means for
143 testing our hypothesis that different levels of cognitive processing and engagement affect how
144 informative and compressible the associated brain patterns are.

145 To evaluate the relation between informativeness and compressibility for brain activity from
146 each experimental condition, we trained a series of across-participant temporal decoders on com-

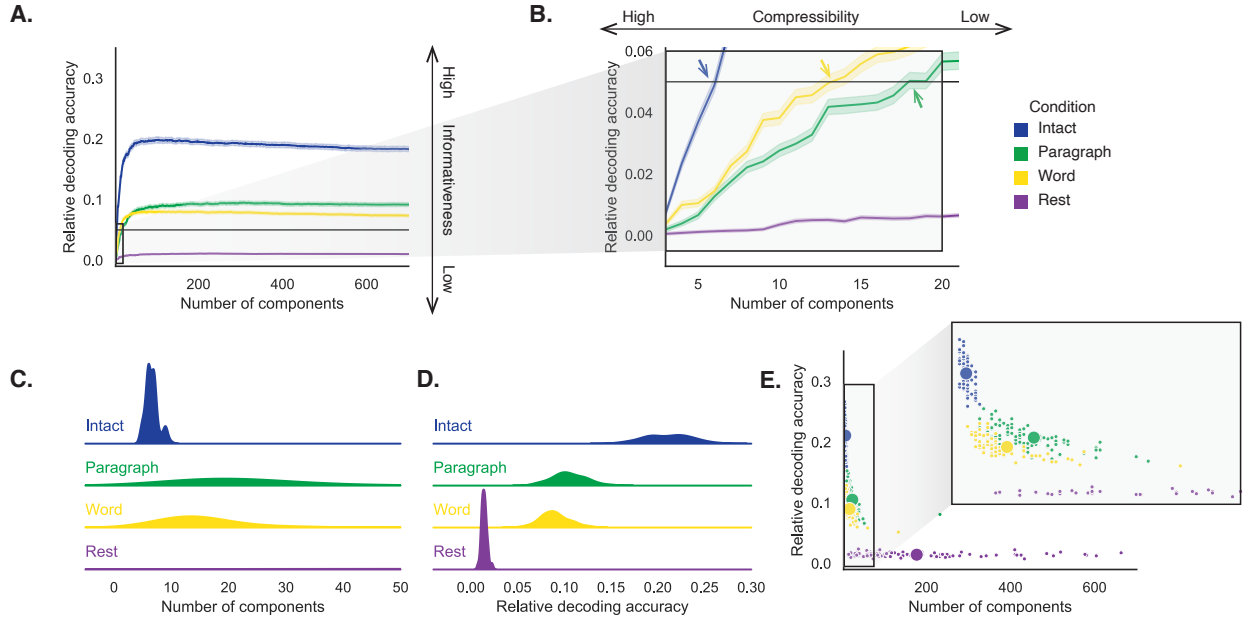


Figure 2: Decoding accuracy and compression. **A. Decoding accuracy by number of components.** Ribbons of each color display cross-validated decoding performance for each condition (intact, paragraph, word, and rest), as a function of the number of components (features) used to represent the data. For each condition, decoding accuracy has been normalized by subtracting expected “chance” decoding performance (estimated as $\frac{1}{T}$, where T is the number of timepoints in the given condition). This normalization was intended to enable fairer comparisons across conditions; a relative decoding accuracy of 0.0 denotes “chance” performance. The horizontal black line denotes 5% decoding accuracy (used as a reference in Panel B). **B. Numbers of components required to reach a fixed decoding accuracy threshold, by condition.** The panel displays a zoomed-in view of the inset in Panel A. Intersections between each condition’s decoding accuracy curve and the 5% decoding accuracy reference line are marked by arrows. All error ribbons in Panels A and B denote bootstrap-estimated 95% confidence intervals. **C. Estimating “compressibility” for each condition.** The density plots display the numbers of components required to reach at least 5% (corrected) decoding accuracy, across all cross validation runs. For the “rest” condition, where decoding accuracy never reached 5% accuracy, we display the distribution of the numbers of components required to achieve the peak decoding accuracy in each fold. (This distribution is nearly flat, as also illustrated in Panel E.) **D. Estimating “informativeness” for each condition.** The density plots display the peak (corrected) decoding accuracies achieved in each condition, across all cross validation runs. **E. Informativeness versus compressibility.** Each dot displays the minimum number of components required to achieve at least 5% corrected decoding accuracy (x -coordinate; for the rest condition the numbers of components are estimated using the peak decoding accuracies as in Panel C) and the peak (corrected) decoding accuracy (y -coordinate). The smaller dots correspond to individual cross validation runs and the larger dots display the averages across runs. The inset displays a zoomed-in view of the indicated region in the main panel.

147 pressed representations of the data. Figure 2A displays the decoding accuracy as a function
148 of the number of principal components used to represent the data (also see Fig. S1). Several
149 patterns were revealed by the analysis. First, in general (i.e., across experimental conditions),
150 decoding accuracy tends to improve as the number of components are increased. However, de-
151 coding accuracy peaked at higher levels for experimental conditions that exposed participants
152 to cognitively richer stimuli (Fig. 2D). The peak decoding accuracy was highest for the “intact”
153 condition (versus paragraph: $t(99) = 35.205, p < 0.001$; versus word: $t(99) = 43.172, p < 0.001$);
154 versus rest: $t(99) = 81.361, p < 0.001$), next highest for the “paragraph” condition (versus word:
155 $t(99) = 6.243, p < 0.001$; versus rest: $t(99) = 50.748, p < 0.001$), and next highest for the “word”
156 condition (versus rest: $t(99) = 48.791, p < 0.001$). This ordering implies that cognitively richer
157 conditions evoke more stable brain activity patterns across people.

158 The cognitively richer conditions also displayed steeper initial slopes. For example, the intact
159 condition decoders reached an arbitrarily chosen threshold of 5% accuracy using fewer components
160 than the paragraph condition decoders ($t(99) = -7.429, p < 0.001$) or word condition decoders
161 ($t(99) = -7.300, p < 0.001$), and decoding accuracy never exceeded 5% for the rest condition. This
162 suggests that brain activity patterns evoked by cognitively richer conditions are more compressible,
163 such that representing the data using the same number of principal components provides more
164 information to the temporal decoders (Figs. 2B, C). Taken together, as shown in Figure 2E, we
165 found that brain activity patterns evoked by cognitively richer conditions tended to be both more
166 informative (i.e., associated with higher peak decoding accuracies) *and* more compressible (i.e.,
167 requiring fewer components to achieve the 5% accuracy threshold).

168 If informativeness (to the temporal decoders) and compressibility vary with the cognitive
169 richness of the stimulus, might these measures also vary over time *within* a given condition? For
170 example, participants in the intact condition might process the ongoing story more deeply later
171 on in the story (compared with earlier in the story) given the additional narrative background
172 and context they had been exposed to by that point. To examine this possibility, we divided each
173 condition into four successive time segments. We computed decoding curves (Fig. 3A) and the
174 numbers of components required to achieve 5% decoding accuracy (Fig. 3B) for each segment and
175 condition. We found that, in the two most cognitively rich conditions (intact and paragraph), both
176 decoding accuracy and compressibility, as reflected by the change in decoding curves, increased

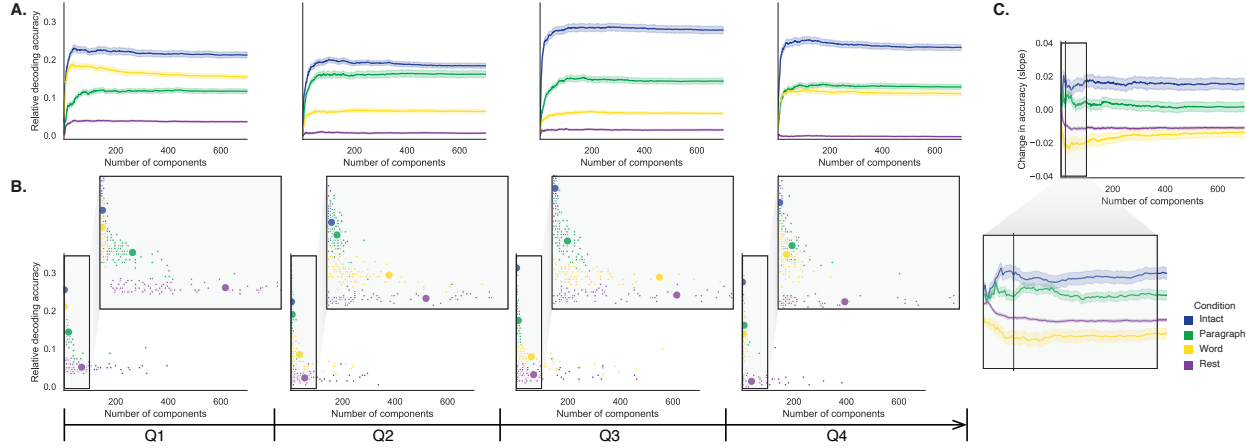


Figure 3: Changes in decoding accuracy and compression over time. **A. Decoding accuracy by number of components, by story segment.** Each family of curves is plotted in the same format as Figure 2A but reflects data only from one quarter of the dataset. **B. Informativeness versus compressibility by condition and segment.** Each scatter plot is in the same format as Figure 2E, but reflects data only from one quarter of the dataset. **C. Change in decoding accuracy over time, by number of components.** For each number of components (x -axis) and condition (color), we fit a regression line to the decoding accuracies obtained for the first, second, third, and fourth quarters of the dataset (corresponding to the columns of Panels A and B). The y -axis denotes the slopes of the regression lines. The black vertical line marks $k = 20$ components, as referenced in the main text. All error ribbons denote bootstrap-estimated 95% confidence intervals.

177 with listening time (e.g., at the annotated reference point of $k = 20$ components in Fig. 3C: intact:
 178 $t(99) = 7.915, p < 0.001$; paragraph: $t(99) = 2.354, p = 0.021$). These changes may reflect an increase
 179 in comprehension or depth of processing with listening time. In contrast, the decoding accuracy
 180 and compressibility *decreased* with listening time in the word condition ($t(99) = -10.747, p < 0.001$)
 181 and rest condition ($t(99) = -22.081, p < 0.001$). This might reflect the depletion of attentional
 182 resources in the less-engaging word and rest conditions.

183 These results make some intuitive sense. As the contextual information available to participants
 184 increases (i.e., over time in the cognitively rich “intact” and “paragraph” conditions), it makes sense
 185 that this might constrain neural responses to a greater extent. While this pattern may not necessarily
 186 hold for *every* possible story or stimulus, we suspect that it is generally the case that our knowledge
 187 about what is happening in a story tends to increase as we experience more about it. In turn, this
 188 could lead to greater consistency in different people’s interpretations of and neural responses to
 189 the stimulus. Similarly, as participants are left to “mind wander,” or as they experience mental
 190 fatigue (i.e., over time in the less cognitively rich “word” and “rest” conditions), we suggest that

191 this might lead to greater variability in neural responses across people, resulting in lower decoding
192 accuracy. Again, it is not necessarily the case that every possible “unengaging” stimulus will lead
193 to greater neural variability as time progresses, but we suspect this phenomenon is likely to hold
194 for a variety of such stimuli. These findings replicate at least to a limited extent (e.g., across
195 both cognitively rich conditions and across both cognitively impoverished conditions, and for the
196 different groups of participants in each of those conditions). However, determining whether these
197 patterns generalize to other stimuli would require additional study (with new stimuli).

198 We also wondered how informativeness and compressibility in the different experimental
199 conditions might vary across brain networks. We used a network parcellation identified by Yeo et
200 al. (2011) to segment the brain into seven distinct networks. The networks can be sorted (roughly)
201 in order from lower-level to higher-level cortex as follows (Figs. 4A–C): visual, somatomotor,
202 dorsal attention, ventral attention, limbic, frontoparietal, and default mode. Next, we computed
203 decoding curves separately for the activity patterns within each network and identified each
204 network’s inflection point, for each experimental condition. Moving from low-order networks
205 to higher-order networks, we found that decoding accuracy tended to increase, particularly in
206 the higher-level experimental conditions (Fig. 4D, E). This suggests that higher-order networks
207 may carry more content-relevant or stimulus-driven “information.” We found no clear trends
208 in the proportions of components required to achieve 5% decoding accuracy across networks or
209 conditions (Fig. 4F).

210 In addition to examining different networks in isolation, we wondered about the general
211 structure of the full-brain (i.e., potentially multi-network) activity patterns reflected by different
212 principal components across different experimental conditions. As shown in Figure 5, we used
213 Neurosynth (Rubin et al., 2017) to identify, for each component, the associations with each of
214 80 themes (see *Reverse inference*). In general, the first principal components across all of the
215 experimental conditions tended to weight most heavily on themes related to cognitive control,
216 memory, language processing, attention, and perception. Other components appeared to vary
217 more across conditions.

218 To gain further insights into which brain functions might be most closely associated with
219 the top-weighted components from each experimental condition, we manually grouped each
220 Neurosynth-derived topic into a smaller set of core cognitive functions. Separately for each com-

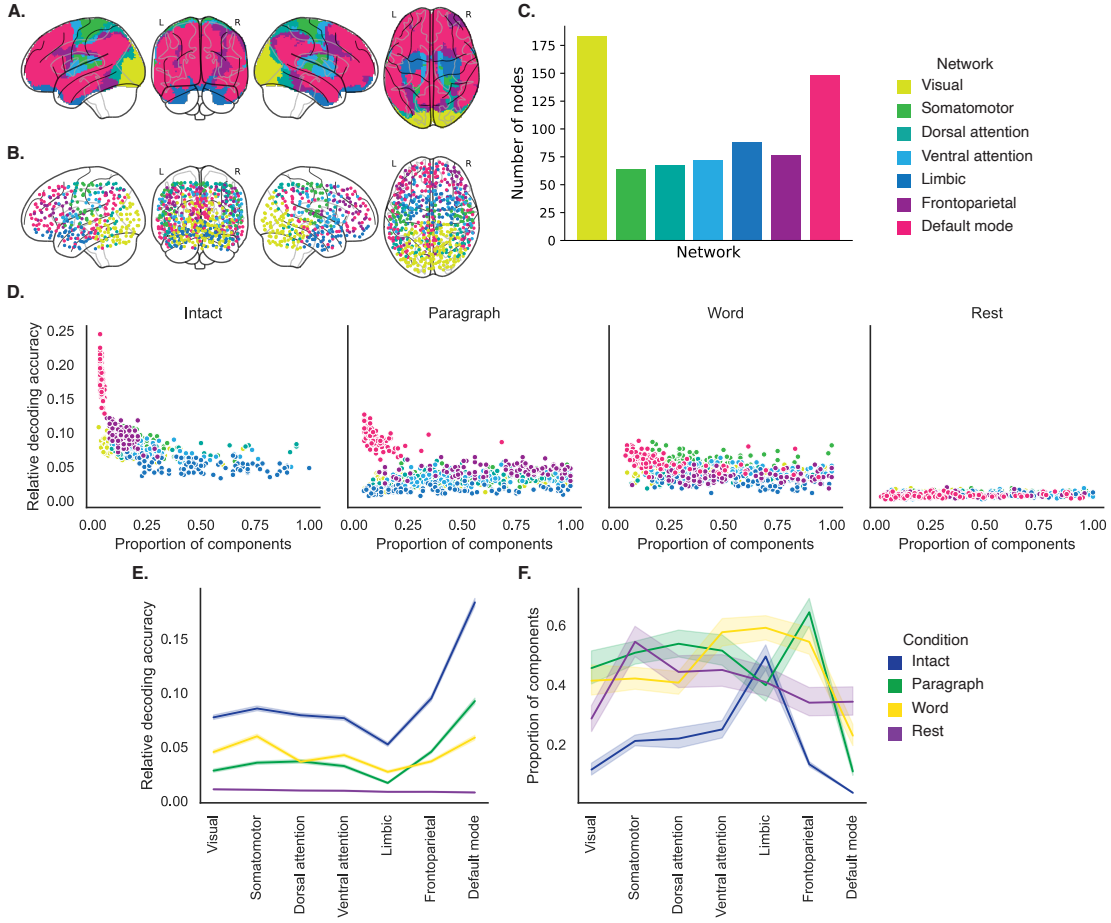


Figure 4: Network-specific decoding accuracy and compression. **A. Network parcellation map.** The glass brain displays the location of each of seven networks identified by Yeo et al. (2011). **B. Node labels.** We assigned network labels to each of 700 Hierarchical Topographic Factor Analysis-derived nodes (see *Hierarchical topographic factor analysis (HTFA)*). For each node, we evaluated its radial basis function (RBF) at the locations of every voxel in the parcellation map displayed in Panel A. We summed up these RBF weights separately for the voxels in each network. We defined each node's network label as its highest-weighted network across all voxels. **C. Per-network node counts.** The bar plot displays the total number of HTFA-derived nodes assigned to each network. **D. Informativeness versus compressibility by network and condition.** Each dot corresponds to a single cross validation run. The dots' coordinates denote the minimum proportion of components (relative to the number of nodes in the given network) required to achieve at least 5% corrected decoding accuracy (x -coordinate; for the rest condition these proportions are estimated using the peak decoding accuracies) and peak (corrected) decoding accuracy (y -coordinate). We repeated the analysis separately for each network (color) and experimental condition (column). **E. Informativeness by network.** For each network, sorted (roughly) from lower-order networks on the left to higher-order networks on the right, the curves display the peak (corrected) decoding accuracy for each experimental condition (color). **F. Compressibility by network.** For each network, the curves display the proportion of components (relative to the total possible number of components displayed in Panel C) required to achieve at least 5% decoding accuracy (or, for the rest condition, peak decoding accuracy, as described above). Error ribbons in Panels E and F denote bootstrap-estimated 95% confidence intervals.

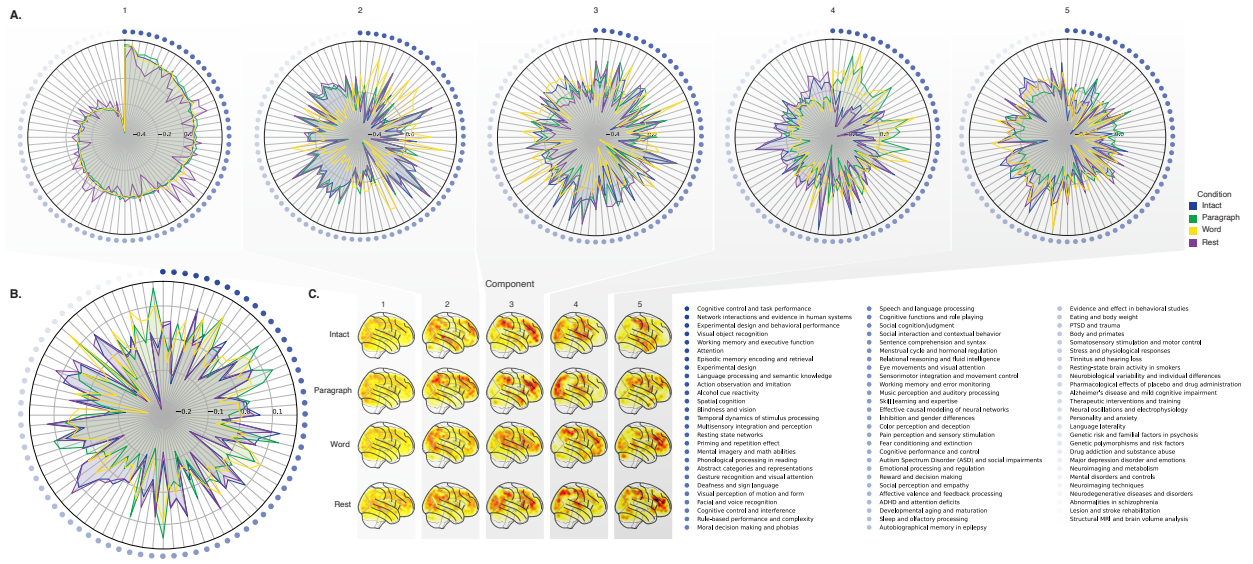


Figure 5: Neurosynth topic weightings by component. We used a reverse inference procedure (see *Reverse inference*) to estimate the correspondences between brain images and a set of 80 topics derived from the Neurosynth database of neuroimaging articles (Rubin et al., 2017). **A. Topic correlations by component.** For each of the top five highest-weighted principal components (columns) derived from each experimental condition (colors), the radar plots display the correlations between the component images and the per-topic images derived for each topic (topic identities are denoted by the blue dots; a legend for the topic labels is in the lower right of the figure). An annotated list of the top-weighted topics for each component and condition may be found in Figure S2 and the top-weighted terms for each topic may be found in Table S1. **B. Topic correlations averaged across components.** The radar plot is in the same format as the plots in Panel A, but here we display the per-condition average correlations across the top five components (for each condition) reflected in Panel A. **C. Component images.** Each plot displays a right sagittal view of a glass brain projection of the top five principal components (columns) for each experimental condition (rows). Additional projections for each component may be found in Figure S3.

ponent, we computed the average weightings across all topics that were tagged as being associated with each of these cognitive functions (Figs. 6A, S5A). To help visualize these associations, we used the patterns of associations for each component to construct graphs whose nodes were experimental conditions and cognitive functions (Figs. 6B, S5B). We also computed correlations between the sets of per-topic weightings from each of the top-weighted components from each experimental condition (Fig. 6C, D) and between the brain maps for each condition's components (Fig. S5C, D). Taken together, we found that each component appeared to weight on a fundamental set of cognitive functions that varied by experimental condition. For example, the top principal components from every condition weighted similarly (across conditions) on the full set of Neurosynth topics (Fig. 5A) and cognitive functions (Figs. 6A, B and S5 A, B), suggesting that these components might reflect a set of functions or activity patterns that are common across all conditions. The second components' weightings were similar across the intact, paragraph, and rest conditions (highest-weighted functions: cognitive control, memory, social cognition, and resting state), but different for the word condition (highest-weighted functions: sensory perception and cognitive control). The fourth components' weighting grouped the paragraph and word conditions (highest-weighted functions: memory, language processing, and cognitive control) and the intact and rest conditions (highest-weighted functions: emotion, social cognition). We also used ChatGPT (OpenAI, 2023) to sort the list of manually tagged cognitive functions from lowest-level to highest-level (Tab. S2, Fig. 6E; also see *Ranking cognitive processes*). We found that higher-level functions tended to be weighted on more heavily by top components from the intact and paragraph conditions than lower-level functions. The top components from the word condition showed the opposite tendency, whereby *lower*-level functions tended to be weighted on more heavily than higher-level functions. The components from the rest condition showed almost no differences in the weights associated with high-level versus low-level functions.

245 Discussion

246 We examined fMRI data collected as participants listened to an auditory recording of a story, scrambled recordings of the story, or underwent a resting state scan. We found that cognitively richer stimuli evoked more reliable (i.e., consistent across people) and information rich brain activity pat-

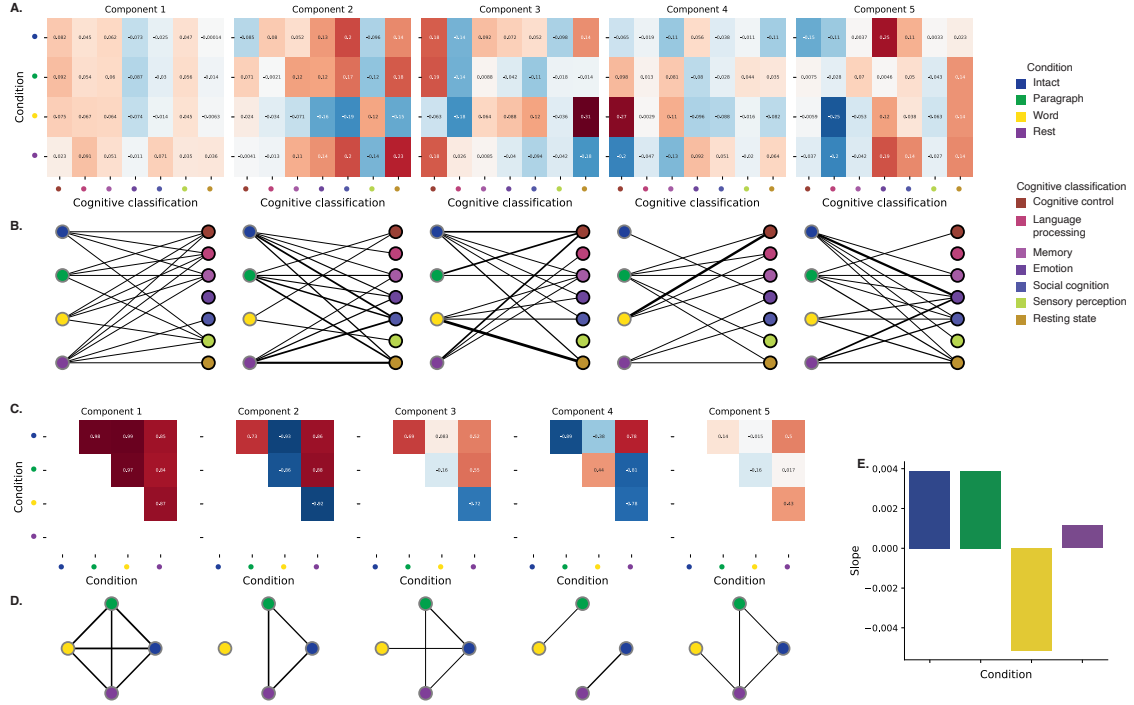


Figure 6: Summary of functions associated with top-weighted components by condition. A. Top-weighted topics by condition. Here we display per-condition (rows, indicated by colored dots) topic correlations, averaged across topics that pertain to each of several broad cognitive functions (columns within each sub-panel, indicated by colored dots). Each sub-panel reflects correlations for the components indicated in the panel titles. A legend for the condition and several core cognitive function classifications is displayed in the lower right of the figure. Table S1 provides a list of each topic's top-weighted terms, along with each topic's manually labeled cognitive classification. A full list of the topics most highly associated with each component may be found in Figure S2. **B. Associations between per-condition components and cognitive functions.** The network plots denote positive average correlations between the component images for each condition (gray-outlined dots on the left sides of each network; colors denote conditions) and topic-specific brain maps associated with each indicated cognitive function (black-outlined dots on the right sides of each network; colors denote cognitive functions). The line thicknesses are proportional to the correlation values (correlation coefficients are noted in the heat maps in Panel A). **C. Correlations between each principal component, by condition.** The heat maps display the correlations between the brain maps (Fig. S3) for each principal component (sub-panel), across each pair of conditions (rows and columns of each sub-panel's matrix, indicated by colored dots). **D. Associations between per-condition components, by component.** Each sub-panel's network plot summarizes the pattern of correlations between the n^{th} top-weighted principal components (sub-panel) for each experimental condition (gray-outlined dots). The line thicknesses are proportional to the correlation values (correlation coefficients are noted in the heat maps in Panel C). **E. Change in weights by condition.** The bar heights reflect the slopes of regression lines, fit separately to the top five components from each condition, between the ChatGPT-derived "rank" of each cognitive classification and the correlations between the component and topic maps associated with cognitive processes at the given rank (see *Ranking cognitive processes*). Also see Fig. S5 for additional information.

249 terns. The brain patterns evoked by cognitively richer stimuli were also more compressible, in that
250 each individual component provided more “signal” to temporal decoders relative to components
251 of data from less cognitively rich conditions (Fig. 2). Over time (e.g., as the experiment progressed),
252 these phenomena were strengthened. Specifically, across story segments, data from more cogni-
253 tively rich conditions became more informative and compressible, and data from less cognitively
254 rich conditions became *less* informative and compressible (Fig. 3). We also repeated these analyses
255 separately for different brain networks. We found that networks traditionally associated with
256 higher-level cognitive functions tended to provide more informative brain patterns than networks
257 traditionally associated with lower level cognitive functions (Fig. 4). Finally, we examined the most
258 dominant components of the brain activity patterns from each experimental condition. We used a
259 reverse inference approach (Rubin et al., 2017) to identify the terms in the neuroimaging literature
260 most commonly associated with the corresponding maps. As summarized in Figure 6E, we found
261 that the intact and paragraph conditions tended to weight on higher-level cognitive processes
262 more than lower-level cognitive processes, whereas the word condition weighted on lower-level
263 processes more than higher-level processes and the rest condition showed no difference in high-
264 level versus low-level weighting. Taken together, our findings indicate that the informativeness
265 and compressibility of our brain activity patterns are task-dependent, and these properties change
266 systematically with factors like cognitive richness and depth of processing.

267 Our explorations of informativeness and compressibility are related to a much broader litera-
268 ture on the correlational and causal structure of brain activity patterns and networks (Adachi et
269 al., 2012; Bassett & Sporns, 2017; Brovelli et al., 2004; Bullmore & Sporns, 2009; Dhamala et al.,
270 2008; Korzeniewska et al., 2008; Lynn & Bassett, 2021; Owen et al., 2021; Preti et al., 2017; Rogers
271 et al., 2007; Rubinov & Sporns, 2010; Sizemore et al., 2018; Smith, Beckmann, et al., 2013; Smith,
272 Vidaurre, et al., 2013; Sporns & Betzel, 2016; Sporns & Honey, 2006; Sporns & Zwi, 2004; Srinivasan
273 et al., 2007; Tomasi & Volkow, 2011; Yeo et al., 2011). Correlations or causal associations between
274 different brain regions simultaneously imply that full-brain activity patterns will be compressible
275 and also that those activity patterns will contain redundancies. For example, the extent to which
276 activity patterns at one brain area can be inferred or predicted from activity patterns at other
277 areas (e.g., Owen et al., 2020; Scangos et al., 2021), reflects overlap in the information available
278 in or represented by those brain areas. If brain patterns in one area are recoverable using brain

279 patterns in another area, then a “signal” used to convey the activity patterns could be compressed
280 by removing the recoverable activity. Predictable (and therefore redundant) brain activity patterns
281 are also more robust to signal corruption. For example, even if the activity patterns at one region
282 are unreadable or unreliable at a given moment, that unreliability could be compensated for by
283 other regions’ activity patterns that were predictive of the unreliable region.

284 Our findings that informativeness and compressibility change with task demands may follow
285 from task-dependent changes in full-brain correlation patterns. A number of prior studies have
286 found that so-called “functional connectivity” (i.e., correlational) patterns vary reliably across
287 tasks, events, and situations (Cole et al., 2014; Owen et al., 2021; Simony et al., 2016; Smith et
288 al., 2009). By examining how these task-dependent changes in correlations affect informativeness
289 and compressibility, our work suggests a potential reason why the statistical structure of brain
290 activity patterns might vary with cognitive task or with cognitive demands. For lower-level tasks,
291 or for tasks that require relatively little “deep” cognitive processing, our brains may optimize
292 activity patterns for robustness and redundancy over expressiveness, for example to maximize
293 reliability. For higher-level tasks, or for tasks that require deeper cognitive processing, our brains
294 may sacrifice some redundancy in favor of greater expressiveness.

295 In the information theory sense (Shannon, 1948), when a signal is transmitted using a fixed
296 alphabet of “symbols,” the information rate decreases as the signal is compressed (e.g., fewer sym-
297 bols transmitted per unit time, using an alphabet with fewer symbols, etc.). Our finding that each
298 individual brain component (symbol) becomes more informative as cognitive richness increases
299 suggests that the “alphabet” of brain activity patterns is also task-dependent. Other work suggests
300 that the representations that are *reflected* by brain activity patterns may also change with task de-
301 mands. For example, our brains may represent the same perceptual stimulus differently depending
302 on which aspects of the stimulus or which combinations of features are task-relevant (Mack et al.,
303 2020).

304 Different brain networks also varied in how informative and compressible their activity pat-
305 terns were across experimental conditions (e.g., Fig. 4). This might follow from evolutionary
306 optimizations that reflect the relevant constraints or demands placed on those networks. One
307 possibility is that cortex is organized in a hierarchy of networks “concerned with” or selective to
308 different levels of processing or function. To the extent that different levels of processing (e.g.,

309 low-level sensory processing versus “deeper” higher-level processing) reflect different stimulus
310 timescales (e.g., Manning, 2020), the network differences we observed might also relate to the
311 timescales at which each network is maximally sensitive (Baldassano et al., 2017; Hasson et al.,
312 2008; Lerner et al., 2011; Regev et al., 2018).

313 **Concluding remarks**

314 Cognitive neuroscientists are still grappling with basic questions about the fundamental “rules”
315 describing how our brains respond, and about how brain activity patterns and the associated
316 underlying cognitive representations and computations are linked. We identified two aspects of
317 brain activity patterns, informativeness and compressibility, that appear to change systematically
318 with task demands and across brain networks. Our work helps to clarify how the “neural code”
319 might be structured, and how the code might vary across tasks and brain areas.

320 **Methods**

321 We measured properties of recorded neuroimaging data under different task conditions that varied
322 systematically in cognitive engagement and depth of processing. We were especially interested in
323 how *informative* and *compressible* the activity patterns were under these different conditions (Fig. 1).

324 Unless otherwise noted, all statistical tests are two-sided, all error bars and error ribbons
325 denote bootstrap-estimated 95% confidence intervals across participants, and all reported *p*-values
326 are corrected for multiple comparisons using the Benjamini-Hochberg procedure (Benjamini &
327 Hochberg, 1995).

328 **Functional neuroimaging data collected during story listening**

329 We examined an fMRI dataset collected by Simony et al. (2016) that the authors have made publicly
330 available at arks.princeton.edu/ark:/88435/dsp015d86p269k. The dataset comprises neuroimaging
331 data collected as participants listened to an audio recording of a story (intact condition; 36 par-
332 ticipants), listened to temporally scrambled recordings of the same story (17 participants in the
333 paragraph-scrambled condition listened to the paragraphs in a randomized order and 36 in the
334 word-scrambled condition listened to the words in a randomized order), or lay resting with their

335 eyes open in the scanner (rest condition; 36 participants). Full neuroimaging details may be found
336 in the original paper for which the data were collected (Simony et al., 2016). Procedures were
337 approved by the Princeton University Committee on Activities Involving Human Subjects, and by
338 the Western Institutional Review Board (Puyallup, WA). All subjects were native English speakers
339 with normal hearing and provided written informed consent.

340 **Hierarchical topographic factor analysis (HTFA)**

341 Following our prior related work, we used HTFA (Manning et al., 2018) to derive a compact
342 representation of the neuroimaging data. In brief, this approach approximates the timeseries
343 of voxel activations (44,415 voxels) using a much smaller number of radial basis function (RBF)
344 nodes (in this case, 700 nodes, as determined by an optimization procedure; Manning et al., 2018).
345 This provides a convenient representation for examining full-brain activity patterns and network
346 dynamics. All of the analyses we carried out on the neuroimaging dataset were performed in
347 this lower-dimensional space. In other words, each participant's data matrix was a number-of-
348 timepoints (T) by 700 matrix of HTFA-derived factor weights (where the row and column labels
349 were matched across participants). Code for carrying out HTFA on fMRI data may be found as
350 part of the BrainIAK toolbox (Capota et al., 2017; Kumar et al., 2021), which may be downloaded
351 at brainiak.org.

352 **Principal components analysis (PCA)**

353 We applied group PCA (Smith et al., 2014) separately to the HTFA-derived representations of the
354 data (i.e., factor loadings) from each experimental condition. Specifically, for each condition, we
355 considered the set of all participants' T by 700 factor weight matrices. We used group PCA to project
356 these 700-dimensional matrices into a series of shared k -dimensional spaces, for $k \in \{3, 4, 5, \dots, 700\}$.
357 This yielded a set of number-of-participants matrices, each with T rows and k columns.

358 **Temporal decoding**

359 We sought to identify neural patterns that reflected participants' ongoing cognitive processing of
360 incoming stimulus information. As reviewed by Simony et al. (2016), one way of homing in on

361 these stimulus-driven neural patterns is to compare activity patterns across individuals. In partic-
362 ular, neural patterns will be similar across individuals to the extent that the neural patterns under
363 consideration are stimulus-driven, and to the extent that the corresponding cognitive representa-
364 tions are reflected in similar spatial patterns across people (Simony & Chang, 2020). Following this
365 logic, we used an across-participant temporal decoding test developed by Manning et al. (2018) to
366 assess the degree to which different neural patterns reflected ongoing stimulus-driven cognitive
367 processing across people. The approach entails using a subset of the data to train a classifier to
368 decode stimulus timepoints (i.e., moments in the story participants listened to) from neural pat-
369 terns. We use decoding (forward inference) accuracy on held-out data, from held-out participants,
370 as a proxy for the extent to which the inputted neural patterns reflected stimulus-driven cognitive
371 processing in a similar way across individuals.

372 **Forward inference and decoding accuracy**

373 We used an across-participant correlation-based classifier to decode which stimulus timepoint
374 matched each timepoint's neural pattern. For a given value of k (i.e., number of principal compo-
375 nents), we first used group PCA to project the data from each condition into a shared k -dimensional
376 space. Next, we divided the participants into two groups: a template group, $\mathcal{G}_{\text{template}}$ (i.e., training
377 data), and a to-be-decoded group, $\mathcal{G}_{\text{decode}}$ (i.e., test data). We averaged the projected data within
378 each group to obtain a single T by k matrix for each group. Next, we correlated the rows of the two
379 averaged matrices to form a T by T decoding matrix, Λ . In this way, the rows of Λ reflected time-
380 points from the template group, while the columns reflected timepoints from the to-be-decoded
381 group. We used Λ to assign temporal labels to each timepoint (row) from the test group's ma-
382 trix, using the row of the training group's matrix with which it was most highly correlated. We
383 repeated this decoding procedure, but using $\mathcal{G}_{\text{decode}}$ as the template group and $\mathcal{G}_{\text{template}}$ as the
384 to-be-decoded group. Given the true timepoint labels (for each group), we defined the decoding
385 accuracy as the average proportion of correctly decoded timepoints, across both groups (where
386 chance performance is $\frac{1}{T}$). In Figures 2 and 3 we report the decoding accuracy for each condition
387 and value of k , averaged across $n = 100$ cross validation folds.

388 **Reverse inference**

389 To help interpret the brain activity patterns we found within the contexts of other studies, we
390 created summary maps of each principal component, for each experimental condition. Each
391 principal component comprises 700 “weights” on each of the HTFA-derived RBF nodes (see
392 *Hierarchical Topographic Factor Analysis*). For each node, we evaluated its RBF at the locations of
393 every voxel in the standard 2 mm MNI152 template brain and multiplied the RBF by the node’s
394 weight. The sum of these weighted RBF activation maps provides a full-brain image, in MNI152
395 space, of the given principal component (Fig. S3).

396 Next, we considered 80 topics estimated using Latent Dirichlet Allocation (Blei et al., 2003)
397 applied to 9,204 functional neuroimaging articles in the Neurosynth database (Rubin et al., 2017).
398 The topics, as well as associated brain maps identified using Neurosynth, were identified and
399 reported in several prior studies (Chen et al., 2020; Fox et al., 2014; Sul et al., 2017). The topic
400 labels for each topic were generated automatically with the following ChatGPT (OpenAI, 2023)
401 prompt: “Please help me come up with intuitive labels for topics I found by fitting a topic model
402 to thousands of neuroscience and psychology articles. I’ll paste in the top 10 highest-weighted
403 words for each topic, and I’d like you to respond with a suggested label. For each topic, please
404 respond with just the topic label and no other formatting or text. Here are the next topic’s top
405 words:” followed by a comma-separated list of the given topic’s top-weighted words reflected
406 in the Table S1. For some topics, ChatGPT responded with a longer-form response rather than a
407 concise topic label. In these instances, on a case-by-case basis, we used a second follow-up prompt
408 to achieve the given topic’s label: “Could you please come up with a more concise label for that
409 topic?”. We then manually identified a set of 11 cognitive labels that were intended to encapsulate
410 a representative range of widely studied low-level and high-level cognitive functions. In choosing
411 the set of cognitive labels, we jointly considered each topic’s ChatGPT-derived topic label, along
412 with the top-weighted words for the topic. We attempted to generate a concise set of labels that
413 still spanned the full set of cognitive functions reflected across the 80 topics. Topics that appeared
414 unrelated to specific cognitive functions (e.g., topics related to specific methods or clinical themes)
415 are designated with dashes in Table S1.

416 Finally, following an approach used in several prior studies (Chen et al., 2020; Fox et al., 2014;

417 Sul et al., 2017) we treated the correlation between a given component’s brain map and each topic’s
418 brain map as an approximate measure of how much the component was reflective of the given
419 topic. This resulted in a set of 80 “weights” (correlation coefficients) for each component’s brain
420 map, with one weight per Neurosynth-derived topic.

421 **Ranking cognitive processes**

422 We manually identified 11 cognitive labels spanning the set of 80 Neurosynth-derived topics:
423 cognitive control, language processing, memory, emotion, social cognition, spatial cognition, at-
424 tention, reward, sensory perception, motor control, and resting state. We then used ChatGPT
425 to automatically “rank” the processes from high-level to low-level using the following prompt:
426 “Please rank these cognitive processes from highest-level to lowest-level, where higher values
427 indicate higher-order or higher-level processes. Return the result as a csv file with a header row
428 and two columns: ‘Cognitive label’ and ‘Rank’. Here are the processes: cognitive control, lan-
429 guage processing, memory, emotion, social cognition, spatial cognition, attention, reward, sensory
430 perception, motor control, resting state”. Table S2 displays the output. We used these labels
431 in the analysis presented in Figure 6E to help summarize difference in topic weightings across
432 experimental conditions.

433 **Synthetic data**

434 To help illustrate the relationship between informativeness and compressibility (Fig. 1), we gen-
435 erated four synthetic datasets, varying in informativeness and compressibility. Each dataset com-
436 prised simulated observations of $K = 25$ features across $N = 100$ timepoints, from each of $S = 10$
437 participants. To create each dataset, we first constructed a “template” matrix of N timepoints by K
438 features. We then generated participant-specific data by adding independent noise to each entry
439 in template matrix, drawn from the unit normal distribution (i.e., with a mean of 0 and a variance
440 of 1). We repeated this process for each participant, yielding S participant-specific matrices for
441 each dataset.

442 Since we estimate informativeness using the temporal decoding accuracy across participants,
443 highly informative data will tend to have observations that are highly timepoint specific. Relatively

444 uninformative data, in contrast, will tend to have more similar observations across timepoints. To
445 generate data with “high informativeness,” we constructed template matrices whose rows (ob-
446 servations) were drawn independently from zero-mean multivariate normal distributions. The
447 covariances of these distributions were determined according to the desired compressibility of
448 the data, as described below. We used a multi-step process to generate data with “low informa-
449 tiveness.” First we generated new template matrices using the same procedure as for the “high
450 informativeness” datasets. We then multiplied each matrix by a constant ($\rho = 0.1$) and computed
451 the cumulative sum of each matrix’s rows. This yielded matrices whose rows were highly similar
452 across observations.

453 Compressibility reflects the extent to which decoding accuracy is affected by reducing the num-
454 ber of components used to represent the data. Highly compressible data will tend to exhibit more
455 similarities across features, whereas less compressible data will tend to show greater independence
456 across features. To generate data with “high compressibility,” we set the covariance matrix of the
457 multivariate normal distribution to a toeplitz matrix whose first row was given by $[K, K - 1, \dots, 1]$.
458 To generate data with “low compressibility,” we set the covariance matrix to the identity matrix.

459 Template matrices for datasets with high informativeness and high compressibility, high in-
460 formativeness and low compressibility, low informativeness and high compressibility, and low
461 informativeness and low compressibility are displayed in Figure 1C. The corresponding decoding
462 curves are displayed in Figure 1D.

463 **Data and code availability**

464 All of the code used to produce the figures and results in this manuscript, along with links to the
465 corresponding data, may be found at github.com/ContextLab/pca_paper.

466 **Acknowledgements**

467 We acknowledge discussions with Rick Betzel, Luke Chang, Emily Finn, and Jim Haxby. Our
468 work was supported in part by NSF CAREER Award Number 2145172 to J.R.M. The content is
469 solely the responsibility of the authors and does not necessarily represent the official views of our

470 supporting organizations. The funders had no role in study design, data collection and analysis,
471 decision to publish, or preparation of the manuscript.

472 **Author contributions**

473 Conceptualization: J.R.M. and L.L.W.O. Methodology: J.R.M. and L.L.W.O. Implementation:
474 J.R.M. and L.L.W.O. Analysis: J.R.M. and L.L.W.O. Writing, Reviewing, and Editing: J.R.M. and
475 L.L.W.O. Funding acquisition: J.R.M. Supervision: J.R.M.

476 **References**

- 477 Adachi, Y., Osada, T., Sporns, O., Watanabe, T., Matsui, T., Miyamoto, K., & Miyashita, Y.
478 (2012). Functional connectivity between anatomically unconnected areas is shaped by collective
479 network-level effects in the macaque cortex. *Cerebral Cortex*, 22(7), 1586–1592.
- 480 Alvarez, S. A. (2002). *An exact analytical relation among recall, precision, and classification accuracy in
481 information retrieval* (Technical Report No. BCCS-02-01). Boston College.
- 482 Baldassano, C., Chen, J., Zadbood, A., Pillow, J. W., Hasson, U., & Norman, K. A. (2017). Discov-
483 ering event structure in continuous narrative perception and memory. *Neuron*, 95(3), 709–721.
- 484 Bassett, D. S., & Sporns, O. (2017). Network neuroscience. *Nature Neuroscience*, 20(3), 353–364.
- 485 Benjamini, Y., & Hochberg, Y. (1995). Controlling the False Discovery Rate: a practical and
486 powerful approach to multiple testing. *Journal of Royal Statistical Society, Series B*, 57, 289–300.
- 487 Blei, D. M., Ng, A. Y., & Jordan, M. I. (2003). Latent dirichlet allocation. *Journal of Machine Learning
488 Research*, 3, 993–1022.
- 489 Brovelli, A., Ding, M., Ledberg, A., Chen, Y., Nakamura, R., & Bressler, S. (2004). Beta oscillations in
490 a large-scale sensorimotor cortical network: directional influences revealed by Granger causality.
491 *Proceedings of the National Academy of Sciences, USA*, 101(26), 9849–9854.
- 492 Bullmore, E., & Sporns, O. (2009). Complex brain networks: graph theoretical analysis of structural
493 and functional systems. *Nature Reviews Neuroscience*, 10(3), 186–198.

- 494 Capota, M., Turek, J., Chen, P.-H., Zhu, X., Manning, J. R., Sundaram, N., ... Shin, Y. S. (2017).
495 *Brain imaging analysis kit.*
- 496 Chen, P.-H. A., Jolly, E., Cheong, J. H., & Chang, L. J. (2020). Intersubject representational
497 similarity analysis reveals individual variations in affective experience when watching erotic
498 movies. *NeuroImage*, 216(116851), doi.org/10.1016/j.neuroimage.2020.116851.
- 499 Cole, M. W., Bassett, D. S., Power, J. D., Braver, T. S., & Petersen, S. E. (2014). Intrinsic and
500 task-evoked network architectures of the human brain. *Neuron*, 83(1), 238–251.
- 501 Dhamala, M., Rangarajan, G., & Ding, M. (2008). Analyzing information flow in brain networks
502 with nonparametric Granger causality. *NeuroImage*, 41(2), 354–362.
- 503 Finn, E. S., Scheinost, D., Finn, D. M., Shen, X., Papademetris, X., & Constable, R. T. (2017).
504 Can brain state be manipulated to emphasize individual differences in functional connectivity.
505 *NeuroImage*, 160, 140–151.
- 506 Finn, E. S., Shen, X., Scheinost, D., Rosenberg, M. D., Huang, J., Chun, M. M., ... Constable, R. T.
507 (2015). Functional connectome fingerprinting: identifying individuals using patterns of brain
508 connectivity. *Nature Neuroscience*, 18, 1664–1671.
- 509 Fox, A. S., Chang, L. J., Gorgolewski, K. J., & Yarkoni, T. (2014). Bridging psychology and
510 genetics using large-scale spatial analysis of neuroimaging and neurogenetic data. *bioRxiv*,
511 doi.org/10.1101/012310.
- 512 Glerean, E., Salmi, J., Lahnakoski, J. M., Jääskeläinen, I. P., & Sams, M. (2012). Functional magnetic
513 resonance imaging phase synchronization as a measure of dynamic functional connectivity.
514 *Brain Connectivity*, 2(2), 91–101.
- 515 Gratton, C., Laumann, T. O., Nielsen, A. N., Greene, D. J., Gordon, E. M., Gilmore, A. W., ...
516 Petersen, S. E. (2018). Functional brain networks are dominated by stable group and individual
517 factors, not cognitive or daily variation. *Neuron*, 98(2), 439–452.
- 518 Hasson, U., Yang, E., Vallines, I., Heeger, D. J., & Rubin, N. (2008). A hierarchy of temporal
519 receptive windows in human cortex. *The Journal of Neuroscience*, 28(10), 2539–2550.

- 520 Korzeniewska, A., Crainiceanu, C. M., Kus, R., Franaszczuk, P. J., & Crone, N. E. (2008). Dynamics
521 of event-related causality in brain electrical activity. *Human Brain Mapping*, 29(10).
- 522 Kumar, M., Anderson, M. J., Antony, J. W., Baldassano, C., Brooks, P. P., Cai, M. B., ... Norman,
523 K. A. (2021). BrainIAK: the brain image analysis kit. *Aperture*, In press.
- 524 Lerner, Y., Honey, C. J., Silbert, L. J., & Hasson, U. (2011). Topographic mapping of a hierarchy of
525 temporal receptive windows using a narrated story. *The Journal of Neuroscience*, 31(8), 2906–2915.
- 526 Lynn, C. W., & Bassett, D. S. (2021). Quantifying the compressibility of complex networks.
527 *Proceedings of the National Academy of Sciences, USA*, 118(32), e2023473118.
- 528 Mack, M. L., Preston, A. R., & Love, B. C. (2020). Ventromedial prefrontal cortex compression during
529 concept learning. *Nature Communications*, 11(46), doi.org/10.1038/s41467-019-13930-8.
- 530 Manning, J. R. (2020). Context reinstatement. In M. J. Kahana & A. D. Wagner (Eds.), *Handbook of
531 human memory*. Oxford University Press.
- 532 Manning, J. R., Zhu, X., Willke, T. L., Ranganath, R., Stachenfeld, K., Hasson, U., ... Norman,
533 K. A. (2018). A probabilistic approach to discovering dynamic full-brain functional connectivity
534 patterns. *NeuroImage*, 180, 243–252.
- 535 Norman, K. A., Polyn, S. M., Detre, G. J., & Haxby, J. V. (2006). Beyond mind-reading: multi-voxel
536 pattern analysis of fMRI data. *Trends in Cognitive Sciences*, 10(9), 424–430.
- 537 OpenAI. (2023, March). *ChatGPT*. Personal communication.
- 538 Owen, L. L. W., Chang, T. H., & Manning, J. R. (2021). High-level cognition during story listening is
539 reflected in high-order dynamic correlations in neural activity patterns. *Nature Communications*,
540 12(5728), doi.org/10.1038/s41467-021-25876-x.
- 541 Owen, L. L. W., Muntianu, T. A., Heusser, A. C., Daly, P., Scangos, K. W., & Manning, J. R. (2020). A
542 Gaussian process model of human electrocorticographic data. *Cerebral Cortex*, 30(10), 5333–5345.
- 543 Preti, M. G., Bolton, T. A. W., & Van De Ville, D. (2017). The dynamic functional connectome:
544 state-of-the-art and perspectives. *NeuroImage*, 160, 41–54.

- 545 Regev, M., Simony, E., Lee, K., Tan, K. M., Chen, J., & Hasson, U. (2018). Propagation of information
546 along the cortical hierarchy as a function of attention while reading and listening to stories.
547 *Cerebral Cortex*.
- 548 Rogers, B. P., Morgan, V. L., Newton, A. T., & Gore, J. C. (2007). Assessing functional connectivity
549 in the human brain by fMRI. *Magnetic Resonance Imaging*, 25(11), 1347–1357.
- 550 Rubin, T. N., Kyojo, O., Gorgolewski, K. J., Jones, M. N., Poldrack, R. A., & Yarkoni, T. (2017).
551 Decoding brain activity using a large-scale probabilistic functional-anatomical atlas of human
552 cognition. *PLoS Computational Biology*, 13(10), e1005649.
- 553 Rubinov, M., & Sporns, O. (2010). Complex network measures of brain connectivity: uses and
554 interpretations. *NeuroImage*, 52, 1059–1069.
- 555 Scangos, K. W., Khambhati, A. N., Daly, P. M., Owen, L. L. W., Manning, J. R., Ambrose, J. B.,
556 ... Chang, E. F. (2021). Biomarkers of depression symptoms defined by direct intracranial
557 neurophysiology. *Frontiers in Human Neuroscience, In press*.
- 558 Shannon, C. E. (1948). A mathematical theory of communication. *Bell System Technical Journal*,
559 27(3), 379–423.
- 560 Simony, E., & Chang, C. (2020). Analysis of stimulus-induced brain dynamics during naturalistic
561 paradigms. *NeuroImage*, 216, 116461.
- 562 Simony, E., Honey, C. J., Chen, J., & Hasson, U. (2016). Dynamic reconfiguration of the default
563 mode network during narrative comprehension. *Nature Communications*, 7(12141), 1–13.
- 564 Sizemore, A. E., Giusti, C., Kahn, A., Vettel, J. M., Betzel, R. F., & Bassett, D. S. (2018). Cliques and
565 cavities in the human connectome. *Journal of Computational Neuroscience*, 44(1), 115–145.
- 566 Smith, S. M., Beckmann, C. F., Andersson, J., Auerbach, E. J., Bijsterbosch, J., Douaud, G., ...
567 Glasser, M. F. (2013). Resting-state fMRI in the Human Connectome Project. *NeuroImage*, 80,
568 144–168.

- 569 Smith, S. M., Fox, P. T., Miller, K. L., Glahn, D. C., Fox, P. M., Mackay, C. E., ... Beckmann,
570 C. F. (2009). Correspondence of the brain's functional architecture during activation and rest.
571 *Proceedings of the National Academy of Sciences, USA*, 106(31), 13040–13045.
- 572 Smith, S. M., Hyvärinen, A., Varoquaux, G., Miller, K. L., & Beckmann, C. F. (2014). Group-PCA
573 for very large fMRI datasets. *NeuroImage*, 101, 738–749.
- 574 Smith, S. M., Vidaurre, D., Beckmann, C. F., Glasser, M. F., Jenkinson, M., Miller, K. L., ... Van
575 Essen, D. C. (2013). Functional connectomics from resting-state fMRI. *Trends in Cognitive Sciences*,
576 17(12), 666–682.
- 577 Sporns, O., & Betzel, R. F. (2016). Modular brain networks. *Annual Review of Psychology*, 67,
578 613–640.
- 579 Sporns, O., & Honey, C. J. (2006). Small worlds inside big brains. *Proceedings of the National Academy
580 of Sciences, USA*, 103(51), 19219–19220.
- 581 Sporns, O., & Zwi, J. D. (2004). The small world of the cerebral cortex. *Neuroinformatics*, 2(2),
582 145–162.
- 583 Srinivasan, R., Winter, W. R., Ding, J., & Nunez, P. L. (2007). EEG and MEG coherence: Measures of
584 functional connectivity at distinct spatial scales of neocortical dynamics. *Journal of Neuroscience
585 Methods*, 166, 41–52.
- 586 Sul, S., Güroğlu, B., Crone, E. A., & Chang, L. J. (2017). Medial prefrontal cortical thinning
587 mediates shifts in other-regarding preferences during adolescence. *Scientific Reports*, 7(8510),
588 doi.org/10.1038/s41598-017-08692-6.
- 589 Tomasi, D., & Volkow, N. D. (2011). Association between functional connectivity hubs and brain
590 networks. *Cerebral Cortex*, 21, 2003–2013.
- 591 Yeo, B. T. T., Krienen, F. M., Sepulcre, J., Sabuncu, M. R., Lashkari, D., Hollinshead, M., ... Buckner,
592 R. L. (2011). The organization of the human cerebral cortex estimated by intrinsic functional
593 connectivity. *Journal of Neurophysiology*, 106(3), 1125–1165.